J Mater Sci (2022) 57:1902–1913

Electronic materials

Dispersing solvent effect on halide perovskite nanocrystals-based films and devices

Fang Chen[1], Yanliang Liu[2], and Marco Salerno[1,3,*]

[1] *Materials Characterization Facility, Istituto Italiano Di Tecnologia, Via Morego 30, 16163 Genova, Italy*
[2] *Shenzhen Institute of Advanced Technology, Chinese Academy of Sciences, Guangdong 518055, China*
[3] *Institute for Globally Distributed Open Research and Education (IGDORE), Genova, Italy*

Received: 8 August 2021
Accepted: 29 November 2021
Published online: 3 January 2022

ABSTRACT

Halide perovskite (HP) nanocrystals (NCs) are promising materials for application in optoelectronic devices. Smooth and compact films, which are obtained by spin coating HP NCs, are required for high-efficiency devices. Whereas solvent plays an important role in spin-coating NCs, there are only few reports on the effect of dispersing solvents of HP NCs films. In this work, a series of solvents with decreasing vapor pressures were used to disperse HP NCs. The resulting morphological and optical properties of the HP NC films were analyzed. It appears that vapor pressure of the solvent and type of solvent have great effect on distribution and optical properties of the HP NCs films. In addition to film characterization, a mixture of two selected solvents was used to fabricate HP NCs-based green LEDs with inorganic electron-transporting materials (ETMs). The reduced leakage and improved LED performance indicate that the mixed solvent helped to stabilize the HP NCs during spin-coating the inorganic ETM. The work suggests that it is important to rationally select the solvent of the HP NCs in order to obtain a compact film and to fabricate efficient LEDs with ETM atop the HP NCs.

Introduction

Halide perovskite (HP) nanocrystals (NCs) have been a hot research topic in recent few years, as they show near-unity photoluminescence (PL) quantum yield, narrow emission width, wide tunable emission wavelengths, large absorption coefficient, and solution processability [1, 2]. These features make HP NCs promising candidates for light emitting devices [3]. For instance, Song et al. [4] have achieved highly efficient HP NC-based LEDs with green emission and external quantum efficiency (EQE) of 21% [5]. Significant progress has also been made in fabricating white light emitting devices based on HP NCs [6–8]

Handling Editor: David Cann.

Address correspondence to E-mail: marco.salerno@iit.it

https://doi.org/10.1007/s10853-021-06777-2

The HP NCs layers used in optoelectronic devices are usually obtained by spin-coating. In order to get HP NCs devices with excellent performance, it is both necessary to optimize the NCs surface by surface engineering [9–13] and to obtain smooth and compact HP NC films [14–17]. Pinholes or uneven distribution of NCs in films could cause current leakage or too high current density in running devices, which leads to low device efficiency [12, 18]. Recently, attention has been paid to this issue, allowing to reach somewhat improved performance [19, 20]. On the way to achieve smooth and compact HP NC films, there are several important conditions to consider [21], such as wettability of substrates [22], proper spin-coating speed [23], ambient humidity, NCs concentration, NCs size, evaporation rates of solvent and types of solvents [24]. Usually, non-polar solvents [25], including toluene [26], hexane [27] and octane [28], are used to disperse HP NCs and to maintain their stability in solution [29]. In some cases, the solvent exerts a significant effect on physical properties of HP NCs. For example, chloroform was demonstrated to passivate bromide vacancies in perovskite thin film [24]. Although there are a plenty of researches about effect of solvents on depositing HP thin films [24, 30, 31] and an amount of investigations about effect of polar solvents on HP NCs during purification [32–34], there has been no report about effect of solvents used for dispersing HP NCs on fabricating HP NC films.

In order to obtain high efficiency, HP NCs-based LEDs usually adopt organic molecules like TPBi [35] as the ETM, which is thermally evaporated onto the NCs layer. However, the organic molecules are expensive and have negative effect on the stability of the LEDs [18]. In contrast, inorganic ETMs like ZnO not only solve the above two problems, but also have higher electron mobility than those of the organic ETMs [36]. However, in spite of its excellent properties, ZnO, which is usually dispersed in polar solvents like ethanol, can damage the NCs as well as wash away the NCs layer during spin-coating process, leading to high current leakage and poor LED performance [37]. To avoid the NCs being washed away while spin-coating ZnO NCs onto the HP NC layer, it is necessary to fix the NCs in the film beforehand.

Here we report on the effect of different dispersing solvents when spin-coating HP NCs films. The solvents were chosen according to their different evaporation rates. The films based on different solvents were characterized in terms of morphology and optical performance. Application of a solvent mixture chosen based on the results of former NCs films characterization demonstrated the possibility of fixing the NCs in the film and fabricating HP NCs-based LEDs with inorganic ETM. The work emphasizes on the significance of rational selection of solvent for dispersing HP NCs in fabrication of HP NC-based optoelectronic devices.

Experimental

Chemicals

Lead acetate trihydrate ($Pb(CH_3COO)_2{\cdot}3H_2O$, 99.99%), cesium carbonate (Cs_2CO_3, reagent Plus, 99%), benzoyl bromide (C_6H_5COBr, 97%, shortly BBr), toluene (anhydrous, 99.5%), octadecene (technical grade, 90%, ODE), oleylamine (70%, OLAM), oleic acid (90%, OA), ethyl acetate (99.8%, EA), diethyl ether (contains BHT as inhibitor, ≥ 99.8%), hexane (anhydrous, 95%), cyclohexane (anhydrous, 99.5%), octane (anhydrous, ≥ 99%), 1,2-dichlorobenzene (anhydrous, 99%), chloroform (≥ 99.5%), and 2,2′,2″-(1,3,5-Benzinetriyl)-tris(1-phenyl-1-H-benzimidazole) (TPBi) were purchased from Sigma-Aldrich. Poly(3,4-ethylenedioxythiophene) polystyrene sulfonate (PEDOT:PSS) was purchased from Ossila. All chemicals were used without any further purification.

Synthesis of HP NCs

The HP NCs were synthesized according to the hot-injection scheme as described by Imran et al. [38], with a minor change of ten times the amount of chemicals. In the synthesis, cesium carbonate (160 mg), lead acetate trihydrate (760 mg), 3 mL of OA, 10 mL of OLAM, and 50 mL of ODE were loaded into a 100-mL 3-neck round-bottom flask and dried under vacuum for 1 h at 130 °C. Subsequently, the temperature was increased to 170 °C under nitrogen flow gradually with air bubbles emerging mildly and moderately, and BBr (700 μL) precursor was swiftly injected into the reaction system. After reacting for 30 s, the reaction mixture was immediately cooled down in an ice-water bath. Finally, degassed toluene (10 mL) was added to the crude

NCs solutions, and the resulting mixture was centrifuged at 4000 rpm for 10 min. The supernatant was discarded, and the precipitate was redispersed in toluene (10 mL) for further use. The measured concentration [39] of the as-synthesized HP NCs, $CsPbBr_3$, is about 180 g/L.

Purification of HP NCs solution

Firstly, 300 µL as-synthesized HP NCs solution was added into a vial. Secondly, 10 µL BBr dispersed in 900 µL EA was added into the vial, and the vial was stirred in glovebox for 10 min. Then, the solutions were transferred to air without opening the lids of the vials and were centrifuged at 5000 rpm for 10 min. Finally, the supernatant was discarded, and the precipitates were re-dispersed in different solvents, including diethyl ether, hexane, cyclohexane, toluene, octane, and 1,2-dichlorobenzene:chloroform (2:1) mixture, for further use. For device fabrication, the solvent mixture was diethyl ether/hexane at a ratio of 1:1, unless otherwise indicated.

Preparation of HP NCs films

Firstly, clean substrates were prepared by rinsing soda-lime glasses with acetone, isopropanol, and Milli-Q water for 10 min in sonication bath in sequence, respectively, and drying under nitrogen flow. Secondly, the HP NCs dispersed in different solvents were spin-coated onto the cleaned glasses at 2000 rpm for 1 min.

Fabrication and characterization of LEDs

LEDs were fabricated on patterned indium-tin oxide (ITO)-coated glass substrates. The substrates were cleaned in an ultrasonic bath using detergent, deionized water, isopropanol and deionized water, sequentially. Prior to depositing the hole-transporting layer, the ITO glass substrates were further treated with oxygen plasma at ~ 0.1 W/cm^2 for 300 s. A PEDOT:PSS layer was then spin-coated onto the cleaned ITO glass substrates at 4000 rpm for 1 min, and the film was annealed in hood at 150 °C for 30 min. Poly-TPD was spin-coated onto the PEDOT:PSS layer at 5000 rpm for 1 min and annealed in glovebox (GB) at 120 °C for 20 min. Here, the poly-TPD solution was prepared in chlorobenzene at 8 g/L in GB. As the film cooled down, the solution of HP NCs dispersed in hexane with and without diethyl ether was spin-coated at 2000 rpm for 1 min and annealed at 70 °C for 15 min [18]. The ZnO NCs solution was spin-coated at 2500 rpm for 1 min onto the HP NCs layer used as ETM [37]. Then, the electrode LiF and Al were thermally evaporated at rate of 0.2 nm/s and 2 nm/s, respectively, up to total nominal thickness of 1.5 and 100 nm, respectively. Finally, the devices were encapsulated with cover glasses and encapsulation oil and treated by UV light for 15 min to solidify the encapsulation oil in GB. The current–voltage–luminance measurement was performed using a Keithley 2410 source-measure unit and an Agilent 34410A multi-meter, coupled to a calibrated PDA 100A Si switchable gain detector from Thorlabs. The output of the Si detector was converted into power (photon flux) using a 50 Ω load resistance and the responsivity of the detector. The EQE was calculated as the ratio of the photon flux and the driving current of the device. The EL spectra of the devices were collected by an Ocean Optics HR4000 + spectrometer.

Characterization techniques

Transmission Electron Microscopy (TEM)

Low-resolution TEM measurements were performed on a JEOL-1100 instrument operating at an acceleration voltage of 100 kV. The HP NCs solutions were drop casted onto carbon-coated copper grids without dilution.

Scanning Electron Microscopy (SEM)

SEM images were recorded by a field emission SEM (Helios NanoLabTM 650), with an acceleration voltage of 2 kV and a filament current of 0.2 A. The as-prepared films were directly used for SEM observation after coating the substrates edges with silver paint.

Confocal PL Microscopy

Confocal PL images and spectra were collected using a Nikon A1 microscopy with a ~ 50 mW laser excitation at 488 nm wavelength. The as-prepared films were directly used for observation.

Light absorption spectra

Light absorption spectra were collected by a Varian Cary 5000 UV –vis –NIR spectrophotometer. The as-prepared films on glasses were directly used for the measurements.

Photoluminescence

Steady-state PL and time resolved PL lifetime were carried out on the films with an Edinburgh fluorescence spectrometer (FLS920). The instrument is equipped with a Xenon lamp and a monochromator for steady-state PL measurement, and a time-correlated single-photon counting unit coupled with a pulsed laser diode (λ = 405 nm, pulse width = 50 ps) for time-resolved PL studies. The steady-state PL was collected with an excitation wavelength of 350 nm.

X-ray Diffraction (XRD)

XRD analysis was performed on a PANanalytical Empyrean X-ray diffractometer, equipped with a 1.8 kW Cu Kα ceramic X-ray tube and a PIXcel3D 2 × 2 area detector, operating at 45 kV and 40 mA. XRD measurements were performed directly on as-prepared films with auto-focus alignment. The diffraction patterns were collected under ambient conditions using parallel beam geometry and symmetric reflection mode. XRD data analysis was conducted using the HighScore 4.1 software from PANanalytical.

Results and discussion

Figure 1 shows TEM images of NCs dispersed in six different solvents. The solvents are diethyl ether, hexane, cyclohexane, toluene, octane, and dichlorobenzene/chloroform, which have increasing boiling points and decreasing vapor pressures (see Table S1). The NCs in different solvents show some difference in distribution on the respective copper grids. In Fig. 1a, one can see NCs with an average size of 7 nm and large particles with an average size of 24 nm (Table S2). The NCs with different sizes evenly spread across the sample; some of the large particles do not follow the distribution trend of the NCs and seem to sit on top of the other NCs, suggesting that these large particles may have formed in the NCs solution. Some large particles follow the natural distribution trend of the surrounding NCs, suggesting in situ chemical sintering among some NCs on the copper grid after deposition of the solution. Figure 1b shows a network of particles with an average size of 19 nm, and NCs with an average size of 8 nm in the background. In the case of cyclohexane (Fig. 1c), the NCs formed several islands with apparent gaps between them. The islands show increasingly darker color from the edge to the center, due to a gradient increase in the NCs size. Apart from the uniform size and homogeneous distribution of the NCs with an average size of 10 nm, in Fig. 1c there are also some NCs with larger size about 17 nm. With respect to the NCs in toluene, the TEM image (Fig. 1d) shows a few dark islands embedded in the orderly distributed NCs with an average size of 8 nm. There are some large particles with clear edges about 12 nm in the dark parts. In the case of NCs in octane (Fig. 1e), apart from a few round dark points with average size of 36 nm, the NCs with an average size of 9 nm generally follow an orderly distribution. With respect to NCs in dichlorobenzene/chloroform (Fig. 1f), there are a few square-shaped objects among the NCs, following the arrangement trend of the surrounding NCs. These squares have an average size of 33 nm, while the NCs have average size of 7 nm. In the darker areas, the distribution of the NCs look blurred, suggesting a mixture of NCs with different sizes. There are also a few white particles in the image, which are attributed to the introduction of BBr during treatment of the pristine NC solution. The TEM images in higher resolution of NCs dispersed in the six different solvents are also given in Fig. S1, which provide some localized NCs distribution information and some details of the NCs.

In general, in each case there are some particles with average size larger than that of the pristine NCs. On one hand, some large particles stochastically spread among the NCs or on the top of the NCs. This may be attributed to a comprehensive effect of reduction of labile ligands on the NCs after being washed with EA and the respective properties of the solvents. On the other hand, some large particles follow the texture of the surrounding NCs. This may be caused by chemical sintering among the NCs after evaporation of the solvents. It is clear that hexane, cyclohexane, and octane show different distribution patterns although the solvents have similar polarities, suggesting some effect of evaporation rates of

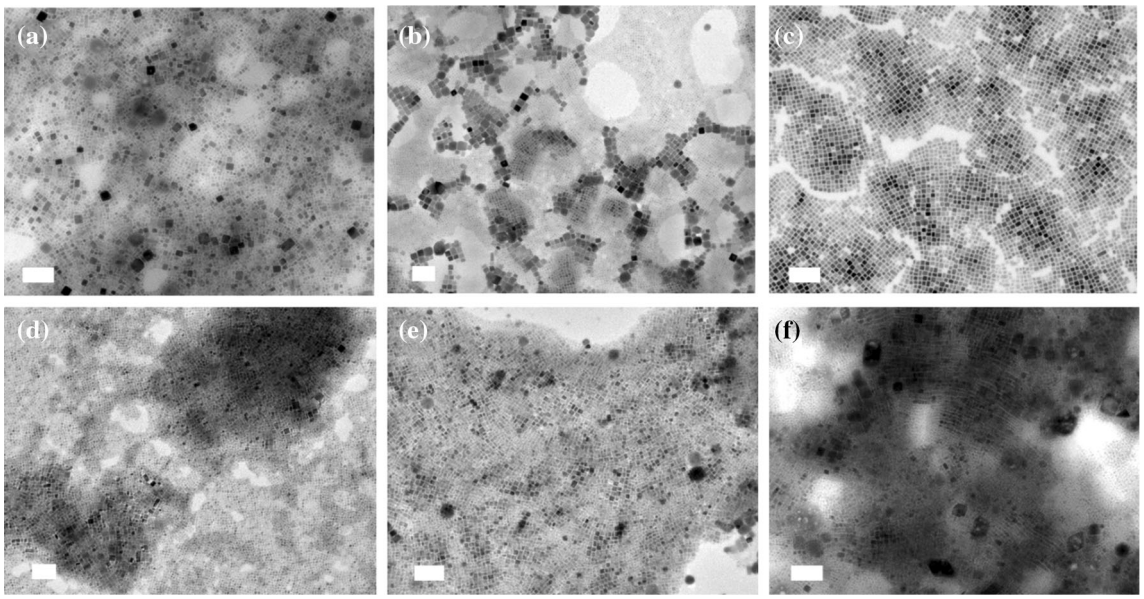

Figure 1 TEM images of HP NCs dispersed in **a** diethyl ether, **b** hexane, **c** cyclohexane, **d** toluene, **e** octane and **f** dichlorobenzene/chloroform (scale bar: 100 nm).

solvents (Table S1) on distribution of the HP NCs on substrates.

Figure 2 presents SEM images of films obtained from NCs solutions with different solvents. Even though SEM images do not provide height information, from the apparent texture of the imaged area we can observe that some films (panels (a), (c). and (f)) look rather smooth, while the others look comparatively rough. The former smooth and generally flat films—apart from a few bumps or uneven areas—originated from diethyl ether, cyclohexane, and dichlorobenzene/chloroform, respectively. In contrast, the latter originated from hexane, toluene, and octane. In particular, in the case of hexane (Fig. 2b),

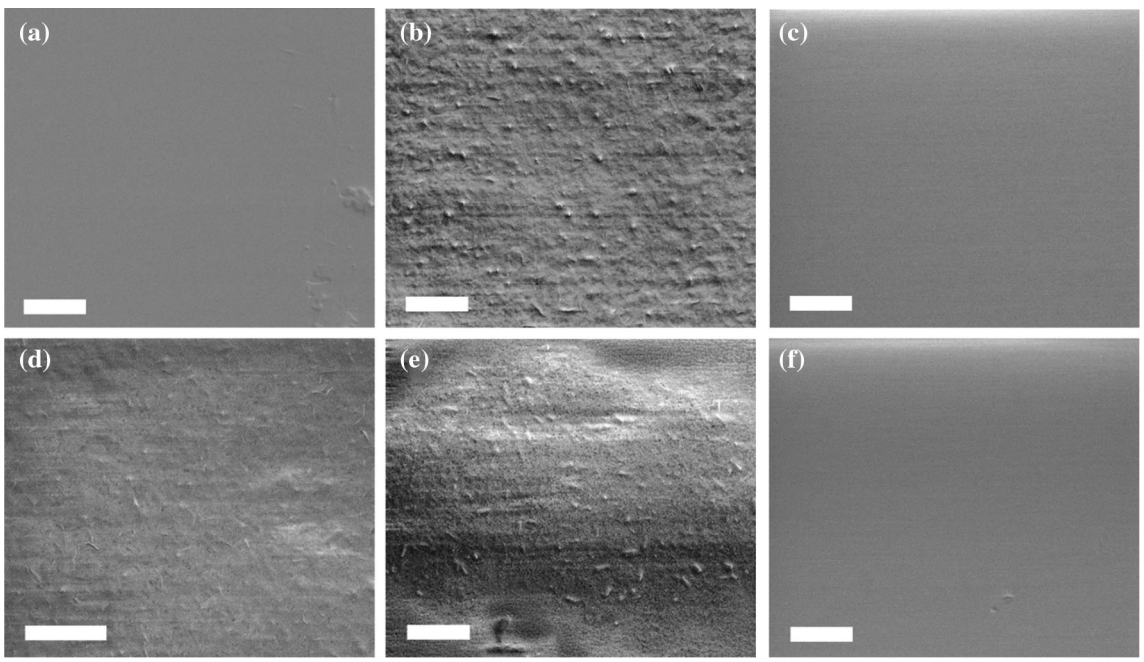

Figure 2 SEM images of HP NC films spin coated from HP NCs dispersed in the series of solvents **a** diethyl ether, **b** hexane, **c** cyclohexane, **d** toluene, **e** octane, and **f** dichlorobenzene/chloroform (scale bar: 10 μm).

there are a plenty of dot-like particles and a few fiber-like particles embedded in the NCs film. In the case of toluene (Fig. 2d), several fiber-like particles emerge that are embedded in the NCs film. At a larger scale, these features appear to be NCs islands (see Fig. S2a, c). For toluene (Fig. 2d), there is another type of area between these islands. As shown in Fig.S2b, large particles appear with an average size of 230 nm, in regions between islands. In the case of octane (Fig. 2e), there are a few bumps formed from the NCs on the glass (see Fig.S3a, d). Within each bump, fiber-like particles can clearly be resolved. Among the bumps, there are networks of NCs (see Fig. S3b). In general, the solvent of NCs has a clear effect on the NCs distribution, driving aggregation to different degrees, and thus on the resulting surface morphology of the NCs films on glass.

The NC films on glass were further characterized by confocal fluorescence microscopy, see Fig. 3. This technique allowed us to identify more clearly the NCs spatial distributions in the films. The brighter regions in Fig. 3 can be associated with the NCs-rich areas at a certain focal plane. Obviously, when looking at the different panels of Fig. 3, one can confirm that films deposited from NCs solutions in different solvents show different spatial distributions of the NCs. For diethyl ether (Fig. 3a), the NCs film appears relatively uniform and compact in spite of some pin-holes (small dark spots) and possible aggregates (large bright spots). In practice, the NCs look like being enwrapped homogeneously in a thick polymer matrix, which is reflected in the clip image from 3D scanning of the confocal fluorescence microscopy (Fig. S4a). Such an apparently thick film is unexpected, considering that diethyl ether has the highest volatility among all considered solvents, due to the highest vapor pressure at room temperature. This suggests strong interaction between diethyl ether molecules and HP NCs, which may be attributed to strong affinity of the latter with the oxygen in diethyl ether. For hexane (Fig. 3b), the NCs film looks also as compact and smooth as in Fig. 3a (no large bright aggregates). For cyclohexane (Fig. 3c), the NCs film shows two levels of brightness associated with branched interpenetrating regions at current focal plane. The contrast may also be partly caused by defocusing at these regions due to relatively high film roughness, as shown by the 3D image (Fig. S4c), even

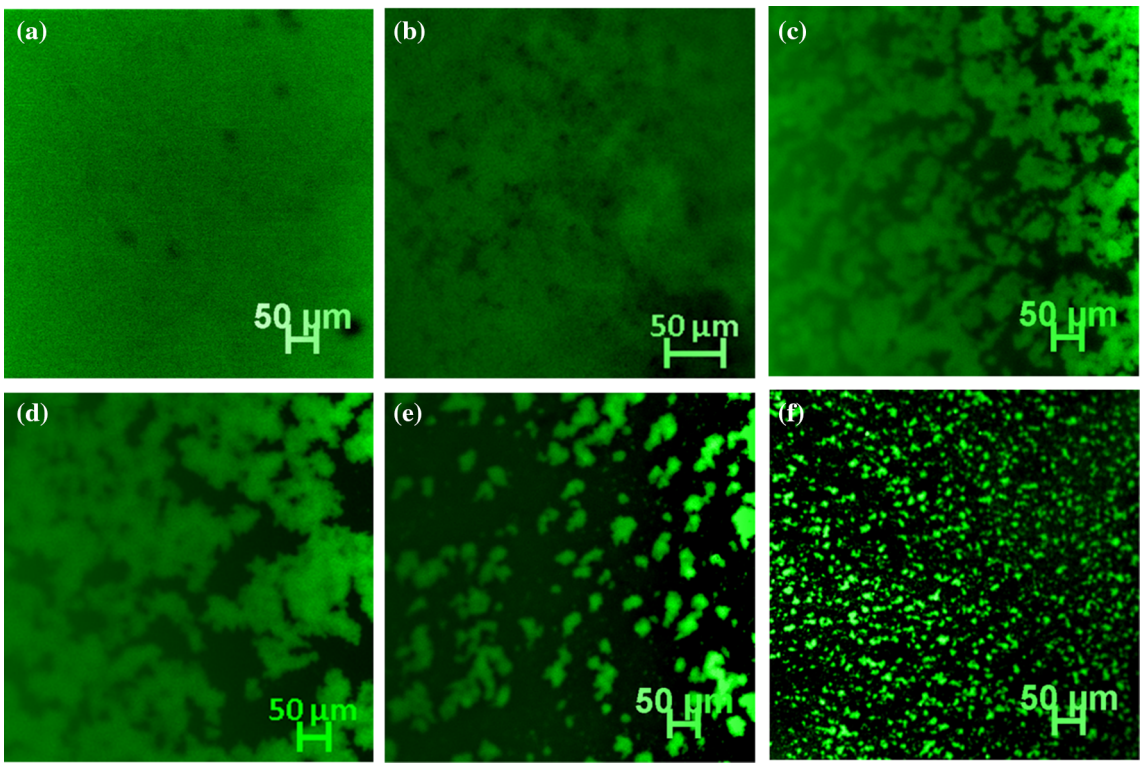

Figure 3 Confocal PL mapping images of HP NC films spin coated from HP NCs dispersed in the series of solvents **a** diethyl ether, **b** hexane, **c** cyclohexane, **d** toluene, **e** octane, and **f** dichlorobenzene/chloroform.

though not apparently confirmed by the respective SEM image (Fig. 2c). For toluene (Fig. 3d), the NCs film also presents a similar pattern as for cyclohexane, with apparently lager interpenetrating black and green regions. Despite this change, the fractal dimension of the images in Fig. 3b-e is not significantly different, staying always in the 2.32–2.36 range, whereas it meets the highest values of 2.47 and 2.53 for the limiting cases of smooth green area in Fig. 3a and uniform distribution of small green islands in Fig. 3f, respectively. According to the 3D image for toluene (Fig. S4d), the black regions in Fig. 3d are seldom covered by NCs, and the film has apparently higher roughness than that for cyclohexane (Fig. 3c). For octane (Fig. 3e), the green region is associated with only a few separated islands, with an average size of 40 μm. Their coverage in this case is as low as ~ 64%, reaching the minimum value of all (whereas the highest coverage of ~ 90 and ~ 95% is observed for Fig. 3a and b, respectively). This is in line with the corresponding 3D image (Fig. S4e), in which the film contains a few bumped islands. It is clear that there are still NCs spreading over the darker area (Fig. S4e), suggesting that the film is uneven and rough. Finally, for dichlorobenzene/chloroform (Fig. 3f), the green areas are associated with much smaller islands, we call them dots, spreading homogeneously throughout the film. Despite the smaller green island size, their coverage increased with respect to the former case, up to ~ 74%. The green islands may be formed by aggregation of the NCs after evaporation of the solvents. The varying sizes of the green islands may be related to interaction, e.g., interface energies, between the NCs and the solvents [40]. Obviously, the solvent does matter for the NCs distribution inside the films obtained on the glass substrates.

In order to understand the effect of solvents on the optical properties of NC films, light absorbance, PL spectra, and PL decay lifetime of the NCs films were characterized. Figure 4a presents the light absorption of the NCs films. It is obvious that light absorption intensities of the NCs films present a wide distribution; nevertheless, interestingly the intensities show a sequential decline from S1 to S6, in line with the descending trend of the vapor pressure of the solvents. Since the concentration of the NCs in each solvent is expected to be the same, and all NCs solutions are spin-coated following the same procedure, the difference in light absorption intensities may only be ascribed to the difference of the vapor pressures of the solvents, which may lead to NC films with different thicknesses. When the spin-coating rate is the same, the higher is the concentration of the NC solutions, the thicker is the film and the stronger is the light absorption. For a solvent with higher vapor pressure, evaporations is faster and the dynamic concentration of the NCs solution increases in a faster manner during the spin-coating process, favoring a thicker film with a stronger UV–Vis light absorption. In contrast, for a solvent with lower vapor pressure, evaporation is slower and the dynamic concentration of the NCs solution increases slower. This may give guidance to determination of best spin-coating parameters. For instance, when the solvent of NCs is changed from hexane to octane, lower spin-coating rate or higher NCs concentration should be used in order to obtain NCs films with similar thicknesses.

Figure 4b shows PL intensities of the NCs films. The PL intensities follow the same trend as the light absorption intensities, except for the first solvent in the series, i.e., diethyl ether. There is also some difference in the PL peaks of the different NCs films. Taking the toluene film as a reference sample, the diethyl ether film shows a little red-shifted PL, while the octane and dichlorobenzene/chloroform films show a little blue-shifted PL (see Fig. S5b). The red-shift in the case of diethyl ether may be due to NCs aggregation or strong self-absorption in the NCs film. The blue-shift for dicholorobenzene/chloroform may be due to a reaction between the NCs and the solvent, since the chlorine in the solvent may partially replace the original bromine on the surface of the NCs [24].

Figure 4c displays the decay lifetimes of the NCs films. The hexane film presents the longest average decay lifetime, 61 ns (Table S3). The decay lifetimes of the other NCs films appear to be of the same order of magnitude. However, the average decay lifetime of diethyl ether is 30 ns, significantly lower than that of the hexane film. This may suggest that diethyl ether introduces more defects into the NCs film. This could also be a reason for the lower PL intensity of diethyl ether film than that of hexane film considering the higher absorption intensity of the diethyl ether film. The octane film displays the shortest average decay lifetime, 15 ns. In general, the dispersing solvent of the HP NCs has a significant effect on the optical performance of the NC films.

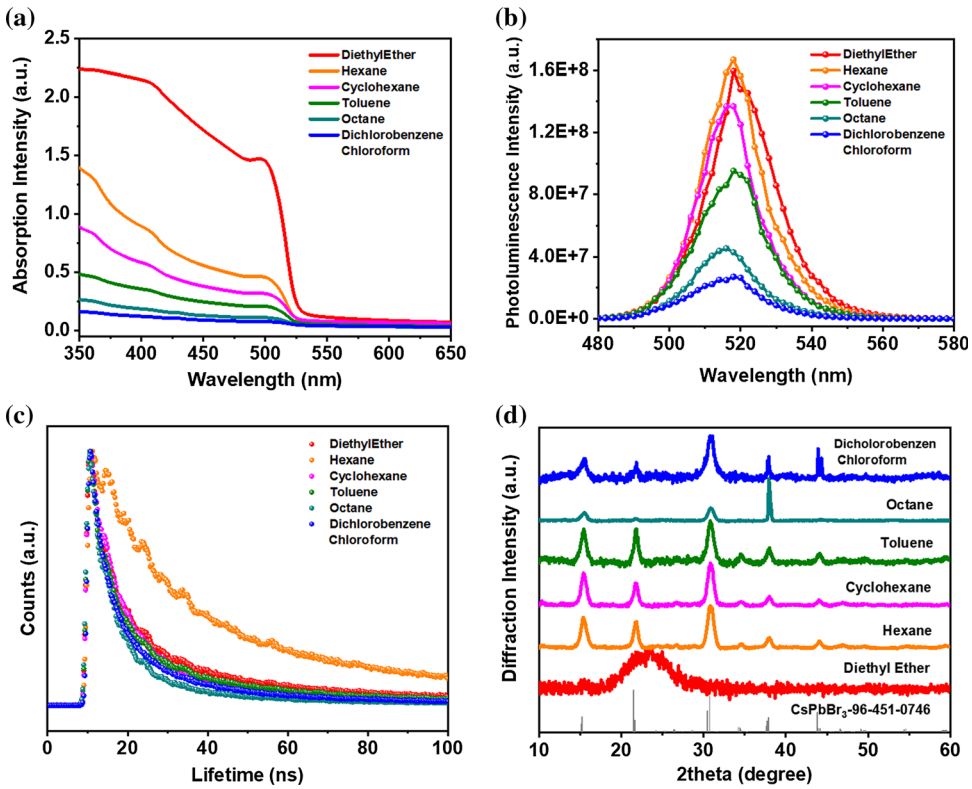

Figure 4 **a** Light absorption spectra; **b** PL spectra; **c** Decay lifetime plots; and **d** XRD patterns of HP NC films spin-coated from HP NCs dispersed in the series of solvents.

In order to see whether the solvent has influence on the phase of the NCs and orientation of the NC films on glass, XRD patterns of the NCs films were collected. As shown in Fig. 4d, all NCs films except those from diethyl ether show similar XRD peaks, matching well with $CsPbBr_3$ with a code of 96-451-0746. The diethyl ether film shows a wide peak around 22°. This may account for the polymer texture of the film. Hexane, cyclohexane and toluene present XRD peaks with almost the same relative intensities. Octane shows a strong diffraction near 37°, which could be attributed to diffraction from (240), (042), (321) and/or (123) planes. Dichlorobenzene/chloroform shows relatively higher peaks near 30°, attributed to (040) and (202) planes, and near 44°, attributed to (242), (400) and (004) planes. The diffraction peaks of films from dichlorobenzene/chloroform are a little broadened relative to the peaks of the other cases, although there is no peak shift. In general, the solvent does not seem to have an obvious effect on the phase of the NCs, but some solvents could lead to preferred orientation with respect to film formation.

The images of the aged NCs solutions and films are displayed in Fig. S6. Obviously, the aged NCs solution in toluene looks brown, while the other NCs solutions still look green. The aged films in sunlight show weakening colors in the series of solvents from diethyl ether to dichlorobenzene/chloroform, and the aged film of the latter solvent is not luminous. Through comparison and combination of different characterization results, it is clear that hexane is the more favorable solvent to form a compact and smooth NCs film with better optical performance on glass substrate. The difference in the NCs films spin-coated from NCs in different dispersing solvents may be attributed to the difference in interaction between solvents and substrates [41], interaction between solvents and ligands on HP NCs [25], and interaction between solvents and HP NCs [26].

According to the above results that the NCs film based on the HP NCs dispersed in diethyl ether look polymer-textured, it is assumed that the NCs may be fixed in the film. Given that nice optical performance is also significant for efficient LEDs, a solvent mixture of diethyl ether and hexane (labeled as W_DE, shortly meaning "with diethyl ether") was prepared and used to disperse the HP NCs. A comparison of the performance of the green LEDs based on the NCs in pure hexane (labeled as WO_DE, shortly meaning "without diethyl ether") and in the W_DE solvent is

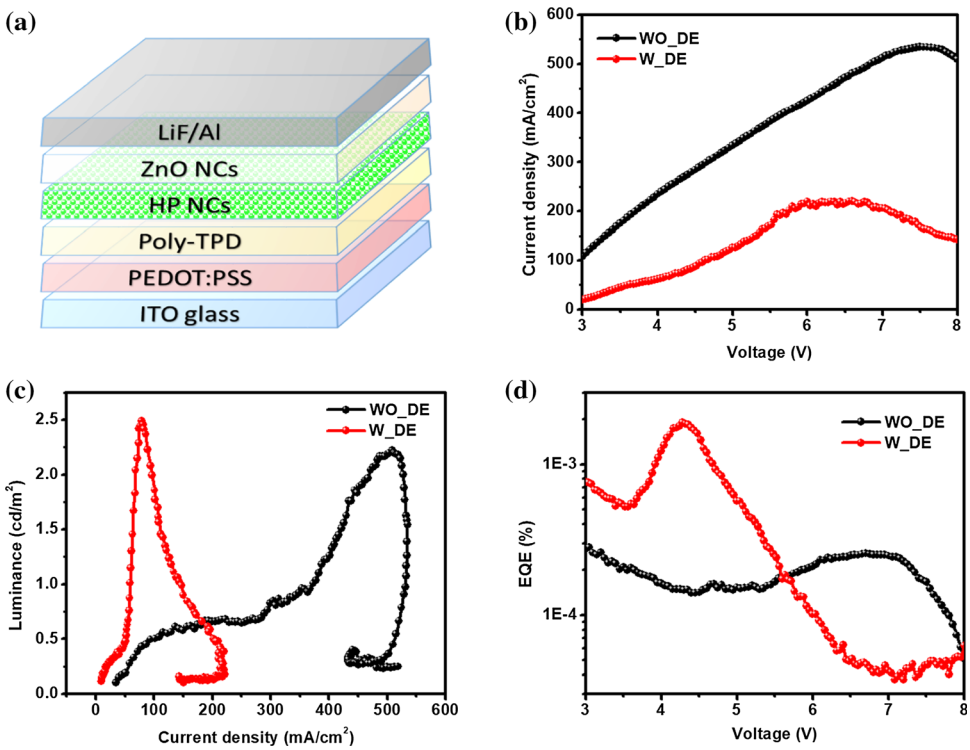

Figure 5 **a** A diagram of the LED structure; **b** Current density as a function of the applied voltage; **c** Luminance as a function of the current density; and **d** EQE as a function of the applied voltage of the WO_DE and W_DE LEDs.

presented in Fig. 5. The LED structure is ITO/PEDOT:PSS/Poly-TPD/HP NCs/ZnO/LiF/Al.

Obviously, the WO_DE LED presents a current density twice to thrice that of the W_DE LED, suggesting less leakage and less damage caused by the ZnO solution in the W_DE LED. In addition, we also prepared LEDs based on NCs dispersed in a series of solutions with ascending ratios of diethyl ether. The current densities of the LEDs exhibit an overall reduction under increasing bias with increasing diethyl ether (Fig. S7), and the overall performance reaches the best when the ratio of diethyl ether/hexane is 1:1. Figure 5c shows that the W_DE LED reaches the highest luminance at a current density of ~ 78 mA/cm^2, while the WO_DE gets the maximum luminance until the current density arrives at ~ 508 mA/cm^2 at a high voltage of 7 V, further indicating serious current leakage in the WO_DE LED. Although the absolute EQEs of the LEDs are low, the higher EQE of the W_DE LED, being more than seven times that of the WO_LED, confirms the positive effect of the addition of diethyl ether in the solvent of the NCs (Fig. 5d). Additionally, also the LEDs with TPBi as ETM, described in the Supplementary Information, present much better performance with the W_DE NCs as the emissive layer (Fig. S8).

Given that there may be an amount of non-radiative defects at the interface of the HP NCs and ZnO NCs, a small amount of TOPO was mixed with the ZnO NC solution and used to optimize the LED performance (Fig. S9). The current density of the LED with TOPO is a bit lower than that of the LED without TOPO, and the luminance increases by about 50%, leading to a 1.5 times higher EQE. As demonstrated by Sun et al. that the solvent of CdSe/ZnS QDs matters for the LED efficiency [42], the current results on LEDs suggest that HP NCs with diethyl ether as a part of solvent may help increase immunity of the HP NCs films to being washed off by polar solvents, and further improve the LED performance with ZnO as ETM.

Conclusion

A series of solvents have been selected and used to disperse HP NCs, in a sequence arranged according to their decreasing vapor pressure. HP NCs films were fabricated by spin-coating HP NCs dispersed in different solvents onto glass substrates. Detailed analysis of the morphology as seen with different techniques, and optical performance of the HP NCs films, showed significant differences among the films.

For the morphology, it was found that diethyl ether dispersing solvent is favorable to form a thick film of HP NCs. Hexane, with a moderate vapor pressure, does well in fabricating smooth and compact HP NCs film with better optical performance than the other cases. With the decrease in vapor pressure of the solvents, the films become thinner and prone to form islands. For the optical properties, it was observed that, when diethyl ether and hexane are mixed as a solvent for the HP NCs, the green LEDs with ZnO NCs as ETM exhibit less current leakage and better performance than LEDs based on NCs merely dispersed in hexane. The work emphasizes on the importance of rational selection of dispersing solvent of HP NCs, in view of improved application of inorganic ETMs in HP NCs-based LEDs as well as in other optoelectronic devices. Future experiments aiming to confirm the effect of solvent vapor pressure could address the kinetics of film formation during spin-coating.

Acknowledgements

Dr. Roman Krahne, Dr. Muhammad Imran, Dr. Milan Palei, Dr. Davide Spirito, and Dr. Beatriz Martin-Garcia are all kindly appreciated for their help with materials and techniques. Dr. Mirko Prato is acknowledged for his useful technical advice. We also wish to thank the Istituto Italiano di Tecnologia for providing access to its facilities.

Declaration

Conflict of interest The authors declare no conflict of interest.

Supplementary Information: The online version contains supplementary material available at https://doi.org/10.1007/s10853-021-06777-2.

References

[1] Akkerman QA, Rainò G, Kovalenko MV, Manna L (2018) Genesis, challenges and opportunities for colloidal lead halide perovskite nanocrystals. Nat Mater 17:394. https://doi.org/10.1038/s41563-018-0018-4

[2] Shamsi J, Urban AS, Imran M, De Trizio L, Manna L (2019) Metal halide perovskite nanocrystals: synthesis, post-synthesis modifications, and their optical properties. Chem Rev 119:3296. https://doi.org/10.1021/acs.chemrev.8b00644

[3] Quan LN, Rand BP, Friend RH, Mhaisalkar SG, Lee T-W, Sargent EH (2019) Perovskites for next-generation optical sources. Chem Rev. https://doi.org/10.1021/acs.chemrev.9b00107

[4] Song J, Fang T, Li J, et al. (2018) Organic-inorganic hybrid passivation enables Perovskite QLEDs with an EQE of 16.48. Adv Mater 30:1805409. https://doi.org/10.1002/adma.201805409

[5] Fang T, Wang T, Li X, Dong Y, Bai S, Song J (2020) Perovskite QLED with an external quantum efficiency of over 21% by modulating electronic transport. Sci Bulletin. https://doi.org/10.1016/j.scib.2020.08.025

[6] Guner T, Demir MM (2018) A review on Halide Perovskites as color conversion layers in white light emitting diode applications. Phys Status Solid (a) 215:1800120. https://doi.org/10.1002/pssa.201800120

[7] Ding N, Zhou D, Sun X et al (2018) Highly stable and water-soluble monodisperse CsPbX3/SiO2 nanocomposites for white-LED and cells imaging. Nanotechnology 29:345703. https://doi.org/10.1088/1361-6528/aac84d

[8] Mei S, Yang B, Wei X et al (2019) Facile synthesis and optical properties of CsPbX3/ZIF-8 composites for wide-color-Gamut display. Nanomaterials 9:832

[9] Pan J, Quan LN, Zhao Y et al (2016) Highly efficient Perovskite-Quantum-dot light-emitting diodes by surface engineering. Adv Mater 28:8718. https://doi.org/10.1002/adma.201600784

[10] Pan J, Shang Y, Yin J et al (2018) Bidentate ligand-passivated CsPbI3 Perovskite nanocrystals for stable near-unity photoluminescence quantum yield and efficient red light-emitting diodes. J Am Chem Soc 140:562. https://doi.org/10.1021/jacs.7b10647

[11] Song J, Li J, Xu L, et al. (2018) Room-temperature triple-ligand surface engineering synergistically boosts ink stability, recombination dynamics, and charge injection toward EQE-11.6% Perovskite QLEDs. Adv Mater 30:1800764. https://doi.org/10.1002/adma.201800764

[12] Chen F, Imran M, Pasquale L, Salerno M, Prato M (2021) Long-term optical and morphological stability of CsPbBr 3 nanocrystal-based films. Mater Res Bull 134:111107. https://doi.org/10.1016/j.materresbull.2020.111107

[13] Xu L, Li J, Cai B et al (2020) A bilateral interfacial passivation strategy promoting efficiency and stability of perovskite quantum dot light-emitting diodes. Nat Commun 11:3902. https://doi.org/10.1038/s41467-020-17633-3

[14] Ban M, Zou Y, Rivett JPH et al (2018) Solution-processed perovskite light emitting diodes with efficiency exceeding 15% through additive-controlled nanostructure tailoring. Nat

Commun 9:3892. https://doi.org/10.1038/s41467-018-06425-5

[15] Xiao Z, Kerner RA, Zhao L et al (2017) Efficient perovskite light-emitting diodes featuring nanometre-sized crystallites. Nat Photonics 11:108. https://doi.org/10.1038/nphoton.2016.269

[16] Wang L, Liu B, Zhao X, Demir HV, Gu H, Sun H (2018) Solvent-assisted surface engineering for high-performance all-inorganic perovskite nanocrystal light-emitting diodes. ACS Appl Mater Interfaces 10:19828. https://doi.org/10.1021/acsami.8b06105

[17] Ochsenbein ST, Krieg F, Shynkarenko Y, Rainò G, Kovalenko MV (2019) Engineering color-stable blue light-emitting diodes with lead halide perovskite nanocrystals. ACS Appl Mater Interfaces 11:21655. https://doi.org/10.1021/acsami.9b02472

[18] Chen F, Boopathi KM, Imran M, Lauciello S, Salerno M (2020) Thiocyanate-treated perovskite-nanocrystal-based light-emitting diodes with insight in efficiency roll-off. Materials 13:367. https://doi.org/10.3390/ma13020367

[19] Shi Y, Wu W, Dong H et al (2018) A strategy for architecture design of crystalline perovskite light-emitting diodes with high performance. Adv Mater 30:1800251. https://doi.org/10.1002/adma.201800251

[20] Chen F, Xu L, Li Y et al (2020) Highly efficient sky-blue light-emitting diodes based on Cu-treated halide perovskite nanocrystals. J Mater Chem C. https://doi.org/10.1039/D0TC03042B

[21] Tyona MD (2013) https://doi.org/10.12989/AMR.2013.2.4.181

[22] Roy S, Ansari KJ, Jampa SSK, Vutukuri P, Mukherjee R (2012) Influence of substrate wettability on the morphology of thin polymer films spin-coated on topographically patterned substrates. ACS Appl Mater Interfaces 4:1887. https://doi.org/10.1021/am300201a

[23] Mohd Arif NAA, Jiun CC, Shaari S (2017) Effect of annealing temperature and spin coating speed on Mn-Doped ZnS nanocrystals thin film by spin coating. J Nanomater 2017:6. https://doi.org/10.1155/2017/2560436

[24] Yu JC, Kim DW, Kim DB et al (2017) Effect of the solvent used for fabrication of perovskite films by solvent dropping on performance of perovskite light-emitting diodes. Nanoscale 9:2088. https://doi.org/10.1039/C6NR08158D

[25] Song J, Li J, Li X, Xu L, Dong Y, Zeng H (2015) Quantum dot light-emitting diodes based on inorganic Perovskite Cesium Lead Halides (CsPbX3). Adv Mater 27:7162. https://doi.org/10.1002/adma.201502567

[26] Krieg F, Ochsenbein ST, Yakunin S et al. (2018) Colloidal CsPbX3 (X = Cl, Br, I) Nanocrystals 2.0: Zwitterionic capping ligands for improved durability and stability. ACS Energy Lett 3: 641. https://doi.org/10.1021/acsenergylett.8b00035

[27] Shi Z, Li Y, Li S et al (2018) Localized surface plasmon enhanced all-inorganic perovskite quantum dot light-emitting diodes based on coaxial core/shell heterojunction architecture. Adv Func Mater 28:1707031. https://doi.org/10.1002/adfm.201707031

[28] Li J, Xu L, Wang T et al (2017) 50-Fold EQE improvement up to 6.27% of solution-processed all-inorganic Perovskite CsPbBr3 QLEDs via surface ligand density control. Adv Mater 29:1603885. https://doi.org/10.1002/adma.201603885

[29] Lou S, Xuan T, Wang J (2019) Stability: A desiderated problem for the lead halide perovskites. Opt Mater X 1:100023. https://doi.org/10.1016/j.omx.2019.100023

[30] Chu Y, Chen Y, Zhou J, Zhou B, Huang J (2019) Efficient and stable perovskite photodetectors based on thiocyanate-assisted film formation. ACS Appl Mater Interfaces 11:14510. https://doi.org/10.1021/acsami.9b01715

[31] Wang W-T, Das SK, Tai Y (2017) Fully ambient-processed perovskite film for perovskite solar cells: effect of solvent polarity on lead iodide. ACS Appl Mater Interfaces 9:10743. https://doi.org/10.1021/acsami.7b01038

[32] Chiba T, Hoshi K, Pu Y-J et al (2017) High-efficiency perovskite quantum-dot light-emitting devices by effective washing process and interfacial energy level alignment. ACS Appl Mater Interfaces 9:18054. https://doi.org/10.1021/acsami.7b03382

[33] Hoshi K, Chiba T, Sato J et al (2018) Purification of perovskite quantum dots using low-dielectric-constant washing solvent "Diglyme" for highly efficient light-emitting devices. ACS Appl Mater Interfaces 10:24607. https://doi.org/10.1021/acsami.8b05954

[34] Kim Y, Yassitepe E, Voznyy O et al (2015) Efficient luminescence from perovskite quantum dot solids. ACS Appl Mater Interfaces 7:25007. https://doi.org/10.1021/acsami.5b09084

[35] Yan F, Demir HV (2019) LEDs using halide perovskite nanocrystal emitters. Nanoscale 11:11402. https://doi.org/10.1039/C9NR03533H

[36] Shi Z, Li S, Li Y et al (2018) Strategy of solution-processed all-inorganic heterostructure for humidity/temperature-stable perovskite quantum dot light-emitting diodes. ACS Nano 12:1462. https://doi.org/10.1021/acsnano.7b07856

[37] Rastogi P, Palazon F, Prato M, Di Stasio F, Krahne R (2018) Enhancing the performance of CdSe/CdS Dot-in-Rod light-emitting diodes via surface ligand modification. ACS Appl Mater Interfaces 10:5665. https://doi.org/10.1021/acsami.7b18780

[38] Imran M, Caligiuri V, Wang M et al (2018) Benzoyl halides as alternative precursors for the colloidal synthesis of lead-

based halide perovskite nanocrystals. J Am Chem Soc 140:2656. https://doi.org/10.1021/jacs.7b13477

[39] De Roo J, Ibáñez M, Geiregat P et al (2016) Highly dynamic ligand binding and light absorption coefficient of cesium lead bromide perovskite nanocrystals. ACS Nano 10:2071. https://doi.org/10.1021/acsnano.5b06295

[40] Abdellatif MH, Abdelrasoul GN, Salerno M et al (2016) Fractal analysis of inter-particle interaction forces in gold nanoparticle aggregates. Colloids Surf A 497:225. https://doi.org/10.1016/j.colsurfa.2016.03.013

[41] Tavana H, Petong N, Hennig A, Grundke K, Neumann AW (2005) Contact angles and coating film thickness. J Adhes 81:29. https://doi.org/10.1080/00218460590904435

[42] Zou Y, Ban M, Cui W et al (2017) A general solvent selection strategy for solution processed quantum dots targeting high performance light-emitting diode. Adv Func Mater 27:1603325. https://doi.org/10.1002/adfm.201603325